University of Nebraska - Lincoln

DigitalCommons@University of Nebraska - Lincoln

Faculty Publications from the Department of Electrical and Computer Engineering

Electrical & Computer Engineering, Department of

3-1-2010

Self assembled nanoparticle aggregates from line focused femtosecond laser ablation

Craig A. Zuhlke
University of Nebraska-Lincoln

Dennis R. Alexander
University of Nebraska-Lincoln, dalexander1@unl.edu

John C. Bruce III
University of Nebraska-Lincoln

Natale J. Ianno
University of Nebraska-Lincoln

Chad A. Kamler
University of Nebraska-Lincoln

See next page for additional authors

Follow this and additional works at: http://digitalcommons.unl.edu/electricalengineeringfacpub

Authors

Craig A. Zuhlke, Dennis R. Alexander, John C. Bruce III, Natale J. Ianno, Chad A. Kamler, and Weiqing Yang

Self assembled nanoparticle aggregates from line focused femtosecond laser ablation

Craig A. Zuhlke, Dennis R. Alexander*, John C. Bruce III, Natale J. Ianno, Chad A. Kamler, and Weiqing Yang

Department of Electrical Engineering, University of Nebraska Lincoln, 844 N 16th St Lincoln, NE 68588, USA
*dalexander1@unl.edu

Abstract: In this paper we present the use of a line focused femtosecond laser beam that is rastered across a 2024 T3 aluminum surface to produce nanoparticles that self assemble into 5-60 micron diameter domed and in some cases sphere-shaped aggregate structures. Each time the laser is rastered over initial aggregates their diameter increases as new layers of nanoparticles self assemble on the surface. The aggregates are thus composed of layers of particles forming discrete layered shells inside of them. When micron size aggregates are removed, using an ultrasonic bath, rings are revealed that have been permanently formed in the sample surface. These rings appear underneath, and extend beyond the physical boundary of the aggregates. The surface is blackened by the formation of these structures and exhibits high light absorption.

References and links

1. N. Singh, D. R. Alexander, J. Schiffern, and D. Doerr, "Femtosecond laser production of metal surfaces having unique surface structures that are broadband absorbers," J. Laser Appl. **18**(3), 242–244 (2006).
2. A. Y. Vorobyev, C. Guo, "Change in absorptance of metals following multi-pulse femtosecond laser ablation," J. of Phy.: Conference Series **59**, 579–584 (2007).
3. A. Y. Vorobyev, and C. Guo, "Enhanced absorptance of gold following multipulse femtosecond laser ablation," Phys. Rev. B **72**(19), 195422 (2005).
4. A. Y. Vorobyev, and C. Guo, "Colorizing metals with femtosecond laser pulses," Appl. Phys. Lett. **92**(4), 041914 (2008).
5. K. Dou, R. L. Parkhill, J. Wu, and E. T. Knobbe, "Surface Microstructuring of Aluminum Alloy 2024 Using Femtosecond Excimer Laser Irradiation," IEEE J. Sel. Top. Quant. **7**(4) (2001).
6. D. Samsonov, and J. Goree, "Particle Growth in a Sputtering Discharge," J. Vac. Sci. Technol. A **17**(5), 2835 (1999).
7. G. M. Robinson, and M. J. Jackson, "Femtosecond Laser Micromachining of Aluminum Surfaces Under Controlled Gas Atmospheres," J. Mater. Eng. Perform. **15**(2), 155–160 (2006).

1. Introduction

Since the advent of the femtosecond laser, its ability to nanomachine, drill and create nanostructures on surfaces has been of great interest. Most of the research on femtosecond laser material surface modification has been conducted using a spherical lens to focus the beam to a spot. A number of pulses are then illuminated on the same spot (e.g., drilling) or the sample is moved so that the laser pulses are rastered across the sample for surface modification and machining [1–4]. Using a cylindrical lens to form a line focused beam to ablate surfaces with a femtosecond laser however, is not as well documented in the literature and is the subject of this paper.

When a beam is focused into a line on a sample, the laser fluence along the line on the surface is much lower than when the same beam is focused to a spot using a spherical lens, with the same minimum spot size dimensions. Using the damage area shown in Fig. 1 (19.8 µm by 4.43 mm) to calculate fluence and comparing this to using a spherical lens that focuses

the beam to a spot 19.8 µm in diameter, the spherical focused beam has a fluence 284 times larger than when a cylindrical lens is used to focus the same amount of energy (same focusing parameters were used for each calculation). A line focus produces a larger but shallower ablation area with each pulse. Furthermore, research conducted in our facilities over the years shows that a line focused beam produces surface modification of materials in a very different way than when using a spherical lens.

When materials are ablated using a femtosecond laser some of the ejected material becomes redeposited on the surface [2–7]. The aggregates discussed in this paper are formed from this redeposited material. Similar aggregates, where nanoparticles combine to form larger structures, have been reported by a number of groups. The Institute of Optics, at the University of Rochester report the growth of aggregates on ablated aluminum, gold and copper samples using a spherical lens to focus a femtosecond laser beam [2–4]. Other groups have also demonstrated similar results [5, 6].

After the 2024 T3 aluminum alloy metal samples are processed using a focused femtosecond line source, they appear black in color. Scanning electron microscope (SEM) analysis shows that the black surface is composed of a large number of dome shaped structures. After the aggregates are removed the surface remains black, although the blackness decreases. Although the blackening of materials using a femtosecond laser processing is not new, we report in this paper for the first time the appearance of aggregates with a discrete layered shell structure. Similar research [1–4] has been conducted using spherical lens for blackening the surface. Previous research by our group has been completed to blacken 2024 T3 aircraft aluminum and gold and the processed samples have been found to be highly absorbing from 0.3 to 50 µm [1]. In this previous work, the structures formed were tens of microns in size, were formed using a spherical lens to focus the laser beam, and had quite different features than those reported in this paper.

2. Experimental setup

A Spectra Physics Spitfire laser system was used as the laser light source. The system is an amplified Ti:sapphire femtosecond laser producing a maximum of 1 mJ of energy in 50 fs pulses at a 1 kHz repetition rate, centered around 800 nm. A 150 mm focal length plano-convex fused silica cylindrical lens was used to focus the output of the femtosecond laser into a line focus onto the surface of the samples. Figure 1 is an SEM image showing damage from a single laser shot using typical parameters used for producing the results in this paper. Figure 1a is a high magnification image showing the width of the resulting ablation spot. Figure 1b is a lower magnification image showing the total length of the ablation spot. The shorter (3.28 mm) measurement marker in Fig. 1(b) is of the area where high surface ablation was observed along the line source ablation using the SEM. The longer (4.43 mm) measurement mark shows maximum damage distance observed along the ablation line source.

A set of Melles Griot nanomotion translation stages, controlled by a computer, were used to translate the sample. Figure 2(a) is a diagram of the experimental setup and Fig. 2(b) is a diagram of the path the stages are programmed to follow when producing the samples discussed in this paper. All samples discussed in this paper were produced on 2024 T3 aluminum.
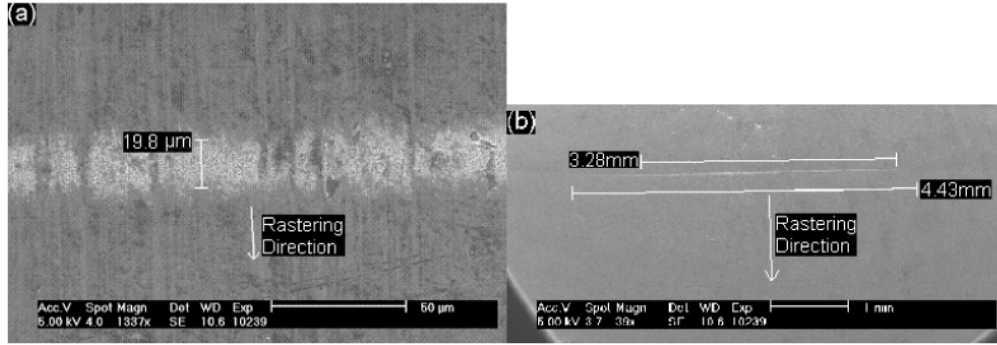
Fig. 1. SEM images of damage to aluminum surface from a single shot. (a) Shows the width of the damage area. (b) Shows the length of the damage area.
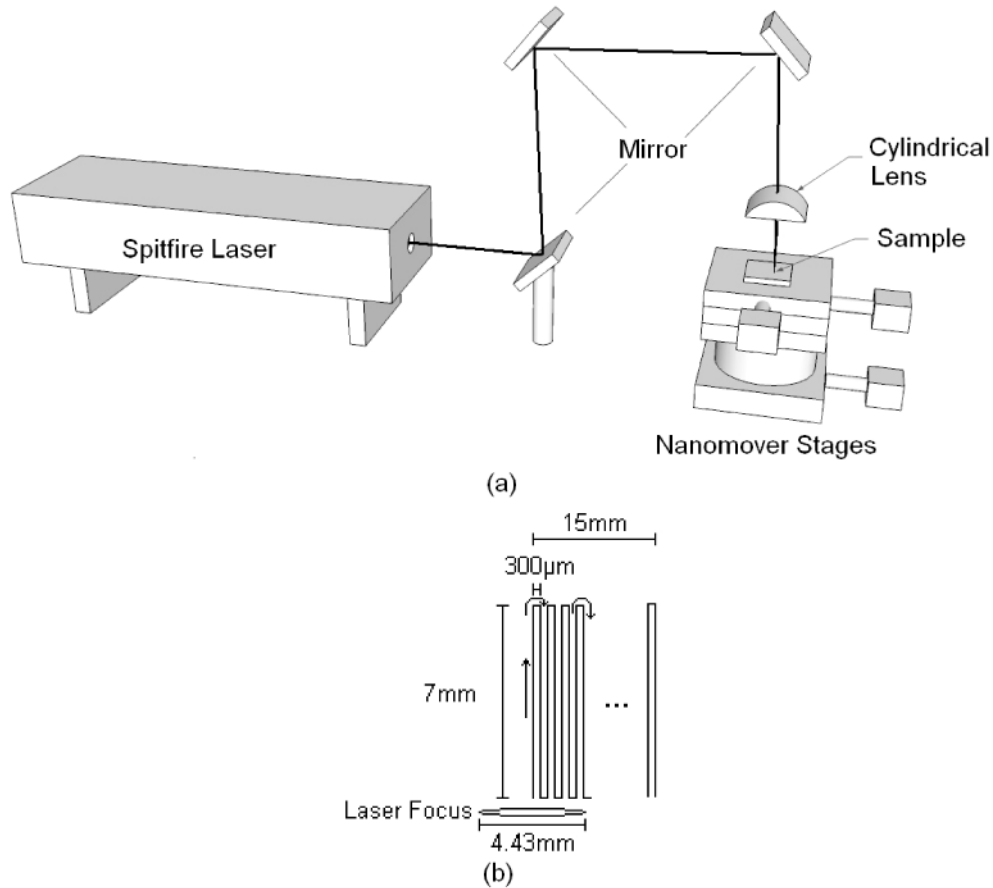

Fig. 2. (a) Experimental setup used in the blackening of the surfaces and the subsequent formation of unique dome shaped structures. (b) Nanomover programmed path used in rastering the surface.

The rastering speed, laser power, and distance between the cylindrical lens and the sample are all parameters that affect aggregate formation. The software used to control the stages was limited to a few discrete translation speeds. It was found that aggregates develop well at 0.5 mm/sec, but do not form at 0.05 mm/sec or 2 mm/sec. Although aggregates can form using a wide range of laser powers, after a series of experiments it was found that 450 µJ/pulse gave the most consistent results. Tests were run that varied the distance between the lens and the

sample and it was found that at 147.4 mm, which is just before the focal length of the lens, the aggregates formed most consistently. There is a window of only about 1 mm in the distance between the cylindrical lens and sample where the aggregates form. Experimentation shows that aggregates will grow if a number of passes are made in the same location, but the rastering path diagrammed in Fig. 2(b) was used in order to create a large number of aggregates over a large area.

For all the samples discussed in this paper the Melles Griot translation stages moved at 0.5 mm/sec, with the spatial path diagramed in Fig. 2(b). The energy was set to 450 µJ/pulse with 50 fs pulses at 1 kHz repetition rate incident upon the cylindrical lens, and the sample surface was located 147.4 mm away from the bottom of the lens. At this height the laser fluence was approximately 0.513 J/cm^2. All images were taken using a Philips XL-30 SEM. It should be noted that when the humidity is in excess of about 35% aggregate growth is negatively affected. So at times, when the humidity in the lab was high experiments were carried out in a chamber with controlled humidity.

3. Results and discussion

Figure 3(a) is an SEM image of aggregates grown on a 2024 T3 aluminum sample. Aggregates preferentially grow on surface defects, but also grow in locations where defects are not visible on the micron scale. When a sample covered in these aggregates is placed in an ultrasonic bath filled with 20°C distilled water for about 1 minute, the aggregates break off. The ultrasonic bath used is a model PC3 by L&R, dissipating 40 Watts at 50 kHz. Figure 3b is an SEM image of aggregates that have broken off, have settled back onto the sample surface, and have been subsequently viewed using the SEM. When a large number of these loose aggregates are collected into a small pile they appear black. Also, individual aggregates look like black dots on a white background surface. Notice the ring structure on the bottom of the center aggregate (Fig. 3(b)). There is also a ring structure that remains on the sample surface and extends beyond the physical boundary of the aggregate after it is removed (Fig. 3(c)).
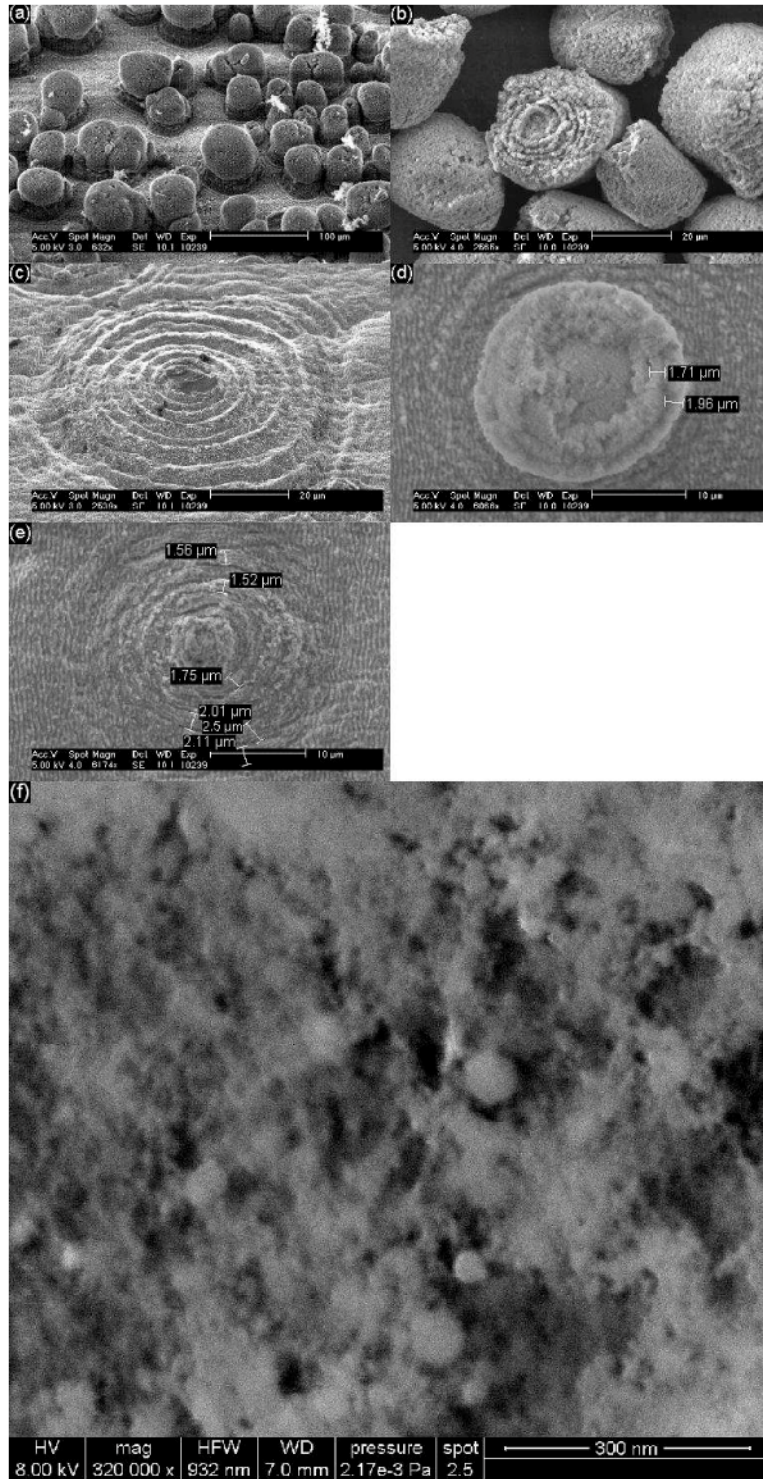
Fig. 3. (a) Spherical aggregates on 2024 T3 aluminum surface. (b) Aggregates that have been removed in an ultrasonic cleaner. (c) Ring structure that has developed under an aggregate. (d) An aggregate with several shells broken open. (e) Image of the ring structure left behind from the aggregate in (d). (f) A high magnification view of the inside of one of the aggregates.

Figures 3(b) and 3(d) illustrate how the aggregates are made up of layers of redeposited nanoparticles that form with each laser pass. In order to cut open an aggregate and expose the inside, a femtosecond laser beam focused with a spherical lens was used to damage some of the aggregates' surfaces. In this particular part of the research study, the femtosecond laser operated at 750 µJ/pulse (800 nm) was focused through a spherical lens with a 125 mm focal length and was rastered across a sample covered with aggregates. This created a damage region 300 µm on each side of the ablation path. Subsequent SEM imaging showed that some of the aggregates' surfaces contained areas of damage; thus allowing the internal structure of the aggregate to be observed. The damage to, and in some cases the complete removal of, aggregates from the surface is due to the shock wave given off from the ablation processes. Figure 3(d) is an image of one of these aggregates with broken shells showing the discrete shell structure. In the SEM image, several layers of shells can be observed along with some markers giving their thicknesses. Figure 3(e) is an image of the ring structure that remains on the surface after the aggregate in Fig. 3(d) was removed. The ring size and shell size are similar in dimensions.

Figure 3(f) is a high magnification view of the inside of one of the aggregates that had been cracked open, similar to the aggregate in Fig. 3(d). It can be seen in the image that the aggregates are a conglomeration of nanoparticles. In the image the larger particles are around 65 nm in diameter and the smaller particles appear to be a few nanometers in diameter.
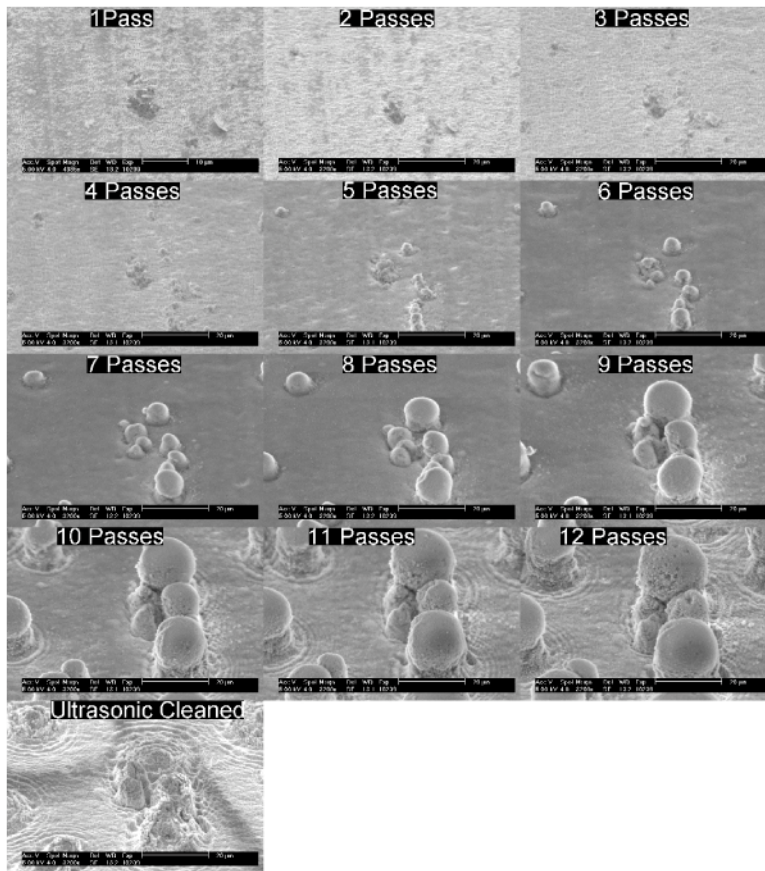

Fig. 4. Progressive set of SEM images of aggregate growth.

In order to better understand the growth of these aggregates, the same experimental setup was used but after each pass the nanomover program was stopped and the surface was

observed in the SEM. Spatial guides were set up on the nanomover stages and in the SEM so the sample could be placed in the same spot after each pass and the same area could be observed.

Figure 4 is a progressive set of SEM images showing growth of aggregates per pass over a single location. From these images it can be seen that with each pass the aggregates increase in size. This stepped growth is a result of ablated nanoparticles redepositing on the aggregate surface from each individual pass.

In a similar experiment, the size of an aggregate was measured in the SEM after each pass. The aggregate was then removed in the ultrasonic cleaner and the diameter of the rings measured in the SEM. The aggregate growth from each pass was found to be similar to the diameter increase of each ring as shown in Fig. 5. When the first measurement was taken a few laser passes had already been made so that the aggregate had already started growing. Growth would be expected to continue if more passes were made across the aggregate. The absolute limits on size were not investigated; however, as passes are made, the density and size of aggregates increases until there is total blockage of the laser pulses reaching the original surface of the material. Remember it is the ablation of the surface that is creating additional nanoparticles leading to aggregate growth with each additional pass of the laser beam. The ring boundaries are defined as the troughs in the permanent ring structure left under the aggregate.
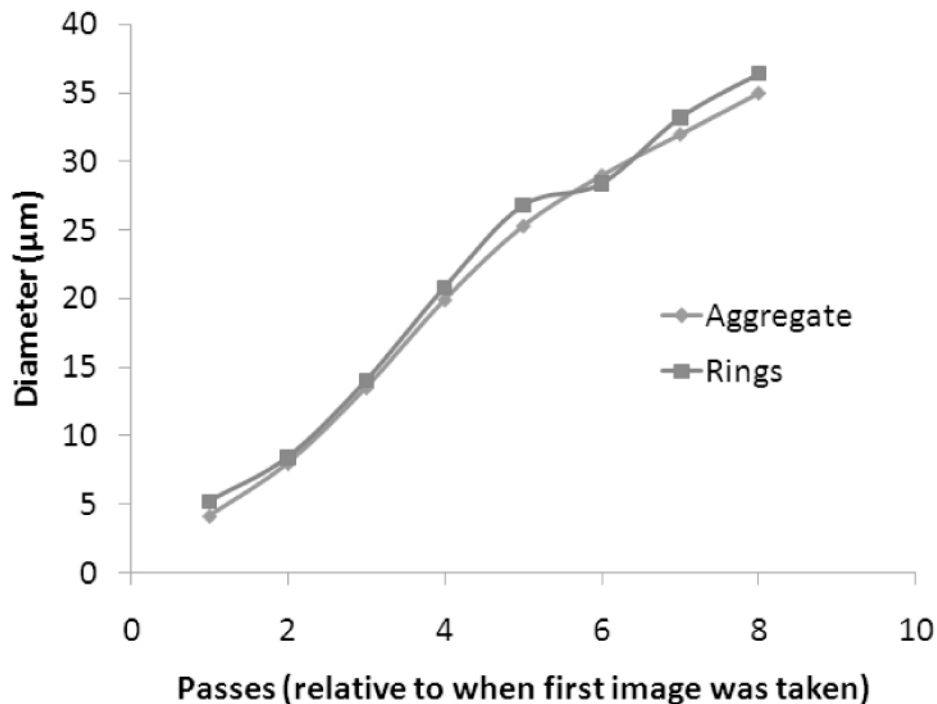

Fig. 5. Plot of aggregate and ring diameters versus the number of laser passes made.

The reason the aggregates do not get ablated away or damaged each time the line focused laser passes over them is a combination of the aggregates growing up from the sample surface so the aggregate surface is out of the laser focus and because of the low fluence from the cylindrical lens. It has been observed in some single pass studies, similar to those described in the previous paragraphs, that after several passes aggregates start to form on the surface. The smaller of these aggregates are ablated away in subsequent passes while the larger aggregates remain and grow even larger.

Once these aggregates grow and become fully established on the surface they do not get ablated away even if the sample height is adjusted so the laser is focused on top of the aggregates. Although surface ablation does occur, the laser fluence resulting from the cylindrical lens line focus is not high enough, and the resulting shock wave is not intense enough to remove aggregates. As a result, with these parameters only the surface of an aggregate can be ablated.

In analyzing the area under and adjacent to an aggregate, there is a polarization dependence that can be observed (see Fig. 6) in the ring structure formed on the sample surface. The incident laser polarization was rotated by 90 degrees between the production of the ring structure shown in Fig. 6(a) and Fig. 6(b). Notice that the area where the ring structure is well defined also rotates 90 degrees (see arrows), and using circularly polarized light the ring structure is similar in all directions. This polarization dependence can be explained by the electric fields due to diffraction being different between directions perpendicular and parallel to the incident laser polarization.
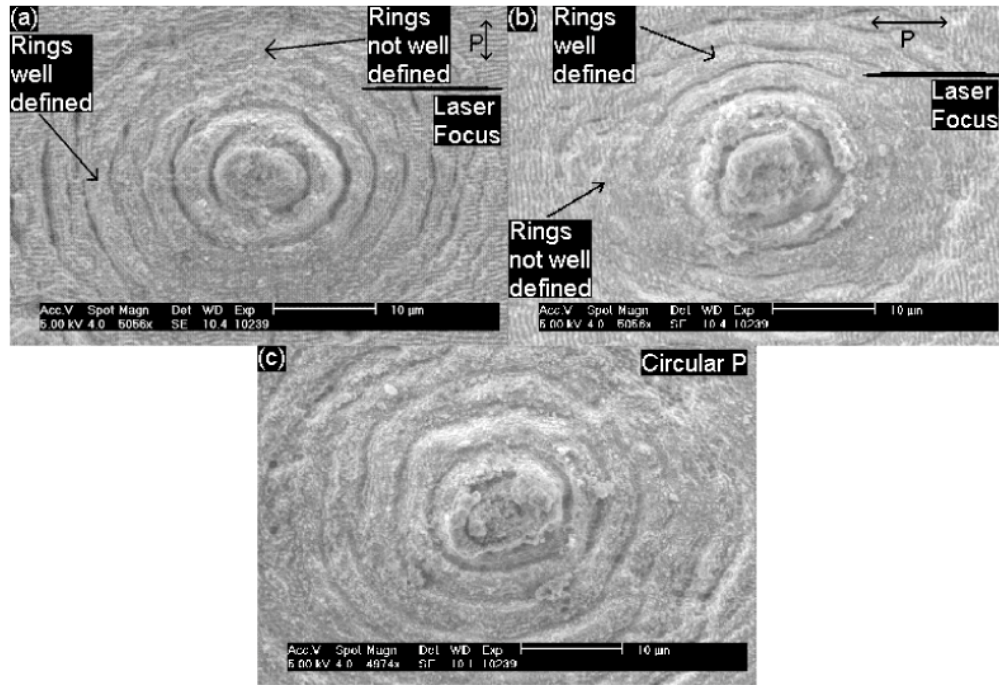

Fig. 6. (a) Linearly polarized in direction shown in image. (b) Linearly polarized in direction shown in image. (c) Circularly polarized.

In order to show this polarization dependence RF Module from COMSOL was used to run finite element analysis of the electric fields that would result from a 20 µm diameter particle that is 10 µm from the sample surface. The problem was simplified to limit resources needed for computation. The aggregate was simplified to be solid aluminum and perfectly spherical. It was also assumed that there was nothing between the aggregate and the surface, the input beam was simplified to a plane wave, and the electric field intensity was 1 V/m. In reality the aggregates are imperfect spheres, are clusters of nanoparticles, and are held away from the surface by clusters of nanoparticles. Also, the width of the line focus along the minimum direction is similar to the size of the aggregate so the intensity profile in this direction would be Gaussian shaped. So the plots are at best good approximations to the experimental situation. The important conclusion to be drawn is that indeed the electric fields differ depending on the laser polarization.
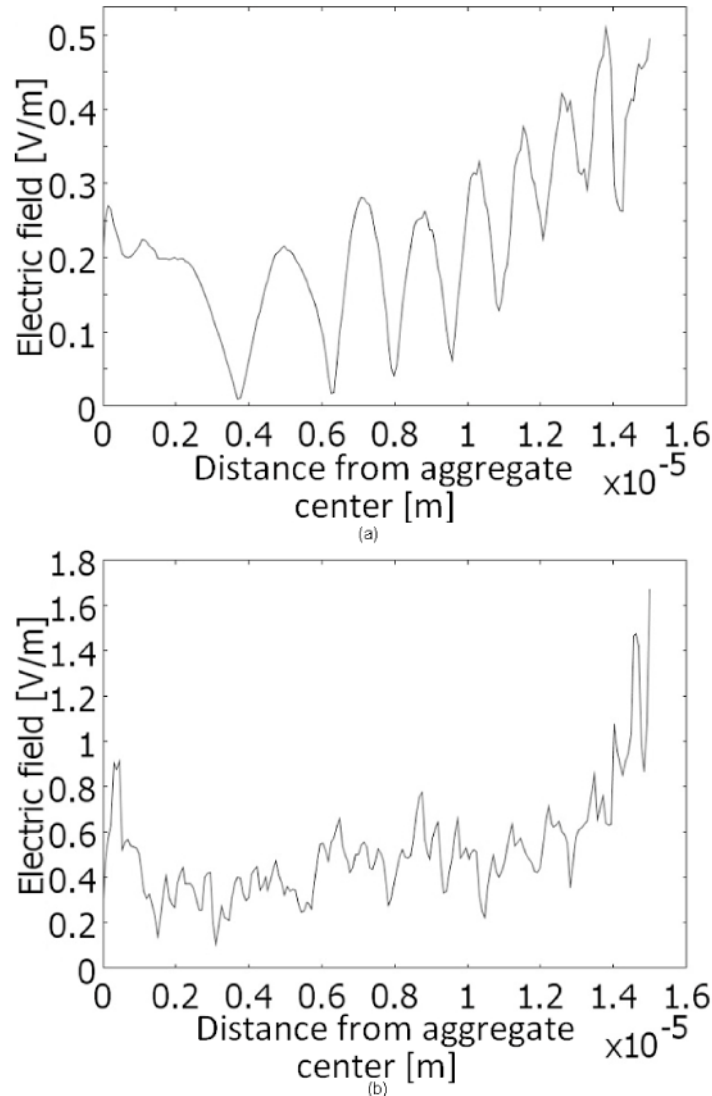
Fig. 7. Simulated electric field intensities near the sample surface scattered by a half sphere of 10 µm radius. The electric field intensities (a) perpendicular and (b) parallel to the input electric field.

Figures 7(a) and (b) are two one dimensional plots for the electric fields that occur 10 nm from the surface. In Fig. 7(a) the incident polarization is perpendicular and in Fig. 7(b) the polarization is parallel. Figure 7(a) is the plot that represents the directions in Fig. 6(a) and (b) where the rings are well defined. It can be seen that in this plot the contrast between the high and low electric field values are greater than in Fig. 7(b) and the peaks are spaced farther apart. We believe this is what causes the better definition in the ring structure that can be seen in Figs. 6(a) and (b). It is important to point out that the non-uniformity of the ring structure is the result of diffraction and is a separate phenomenon from the aggregate growth process. It can be seen in Fig. 7(b) that the intensity peaks are much closer together and there is less defined contrast between the high and low values, and so the ablation caused by the electric field maxima may overlap.

The ring formation that remains on the surface after the aggregates are removed, comes from a combination of shell growth after each pass and diffraction effects. The rings directly

under aggregates, which have several shells assembled on them, form because there is a diffraction peak at the edge of the aggregate. This leads to a high ablation area occurring at the edge of the aggregate with each new shell. The addition of a new shell after each pass causes this ablation ring to be increased the same amount as the aggregate diameter is increased. The rings that form outside of the shadow of the aggregate are purely due to diffraction.
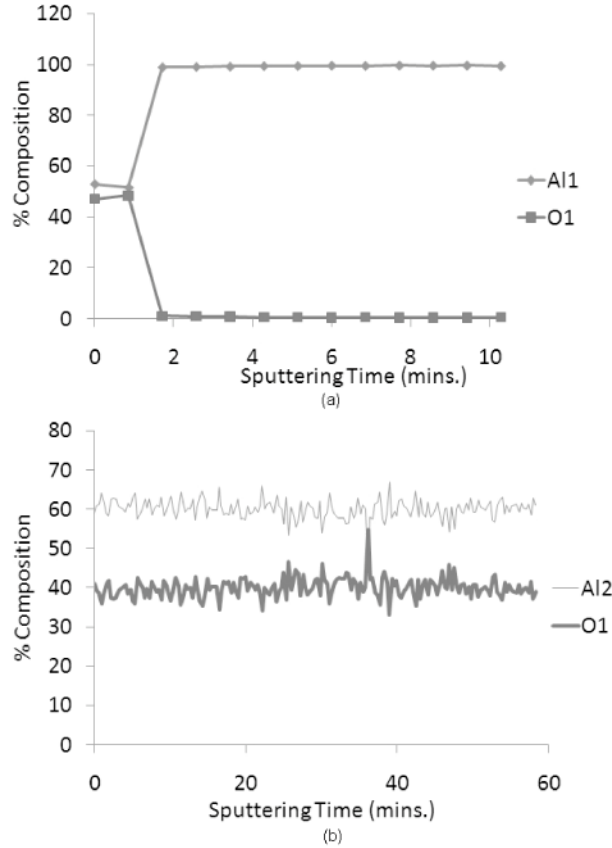

Fig. 8. Auger plots of elemental composition for (a) an unablated sample (b) a sample covered in aggregates.

In an effort to understand the composition of the aggregates, a PHI 560 AES/XPS Auger spectroscopy system was used to analyze the elemental makeup of the sample being ablated and of the aggregates. The system was set to continuously probe as the sample was ion beam milled to prevent reoxidation of the sample surface. The electron beam was set to 3 keV with an emission current of 105 µA, and the ion beam was set to 3 keV with an emission current of 25 mA.

Results for an unablated sample of aluminum are shown in Fig. 8(a) and results for aggregates are shown in Fig. 8(b). It can be seen in Fig. 8(a) that for an unablated sample the ratio of oxygen to aluminum quickly decreases as the ion beam mills away more of the target surface. However, from Fig. 8(b) it can be seen that when the sample containing the aggregates is analyzed, the oxygen and aluminum ratios stay relatively constant versus depth of analysis. These results corroborate that the aggregates are made up of nanoparticles each covered with an oxide layer. When the aggregate sample was analyzed the 1396 eV, Al2 line was used instead of the 68 eV, Al1 line because the oxidation of aluminum causes its first line to shift decreasing the measurement accuracy. The oxygen line used was the 510 eV, O1 line.

As mentioned in the introduction, other groups have reported the blackening of a surface using a spherical lens to focus a femtosecond laser. Our research group has produced aggregates similar to those discussed in this paper on aluminum 2024 T3 with the use of a spherical lens and by rastering the laser across the sample, but they were not quite as dome shaped and there was no evidence of ring structure reported in this work [1]. We have also observed that when a spherical lens is used to ablate a single spot using many laser pulses, aggregates can develop in the recast region outside of the ablation spot. Other groups have reported similar results [3–5]. However, the domed aggregates that develop using a spherical lens do not develop nearly as well as when using a cylindrical lens and are generally not as dense. Continuously passing over a region covered with aggregates with a focused femtosecond line source causes the aggregates to grow larger and new aggregates to develop at additional locations. With a sufficient number of passes the sample surface becomes completely covered with these aggregates. The surface blackness depends on the density of the aggregates. The surfaces are highly absorbing of radiation over a wide spectrum of wavelengths [1].

4. Conclusion

We have demonstrated how a cylindrical lens can be used to produce nanostructured micron size aggregates with a 5-60 µm diameter on 2024 T3 aluminum sample. Aggregates increase in size each time the laser is passed over them as ablated plume nanoparticles self assemble on their surface. As a result permanent ring structures develop inside the aggregates' bodies. The processed surfaces are black in color with both the surfaces and the aggregates consisting of the same oxide material. Since these micron size aggregates are made up of nanoparticles they are very porous and have a high surface area. These unique ring structured aggregates could prove to be useful in a number of applications including high surface area electrodes for ultracapacitors, optical stealth surfaces, and increased thermal emissivity. A focused line source optimizes the formation of aggregate growth and the blackening of a surface. This increased rate of blackening has important applications for large area surface modifications of metals and semiconductor materials.

Acknowledgments